JOURNAL OF THERMOPHYSICS AND HEAT TRANSFER
Vol. 17, No. 1, January–March 2003

Parallel Computation of Fully Coupled Hypersonic Radiating Flowfield Using Multiband Model

Shingo Matsuyama,* Takeharu Sakai,† Akihiro Sasoh,‡ and Keisuke Sawada§
Tohoku University, Sendai 980-8579, Japan

Parallel computation of a fully coupled, strongly radiating hypersonic flowfield is carried out. A detailed multiband model is used in the radiation calculation. The radiative heat flux is calculated using one- (tangent-slab) or two-dimensional approximations in radiative transfer, or by considering three-dimensional radiative transfer directly. To reduce the vast computing time due to a spectrally detailed and multidimensional radiation calculation, a parallel computation is employed. The strategy in the parallel implementation of the code is to divide the wavelength range in the multiband model into groups of the same number of available processors, instead of dividing the computational domain. Calculations are carried out for the flowfield over hemispheres at a speed of 15.24 km/s and an altitude of 57.9 km. The computed results are compared with those obtained in previous studies. A fair agreement of the shock standoff distance with the existing results is shown for several different radii. However, the present result gives a substantially larger radiative heat flux value at the stagnation point for smaller radius cases. This is because the radiative heat transfer from the wavelength region shorter than 1400 Å is found to be optically thick in the shock layer and becomes dominant in these smaller radius cases. The parallel code developed in the present study achieves a computational speed of approximately 20 giga-floating point operations per second using 128 processors on the SGI ORIGIN 2000. The converged solutions for strongly radiating flowfield can be obtained within a feasible computing time.

Nomenclature

F	=	x component of convective flux vector
G	=	y component of convective flux vector
$\boldsymbol{H}$	=	source vector for axisymmetric flow
$\boldsymbol{H}_{\text{rad}}$	=	source vector for radiation
n_i	=	number density of species i, mol/m^3
Q	=	conservative variable
q_{rad}	=	radiative heat flux, W/cm^2
q_λ	=	spectral radiative heat flux at wavelength λ, W/(cm$^2 \cdot \mu$m)
T	=	temperature, K
κ_λ	=	absorption coefficient at wavelength λ, m^{-1}
λ	=	wavelength, Å
σ_λ^i	=	absorption cross section of species i at wavelength λ, m^2/mol

Subscripts

i	=	chemical species i, or ith processor
λ	=	wavelength

Superscript

i	=	chemical species i

Presented as Paper 2001-0657 at the AIAA 39th Aerospace Sciences Meeting, Reno, NV, 8–11 January 2001; received 18 January 2002; revision received 5 August 2002; accepted for publication 13 August 2002.

*Graduate Student, Department of Aeronautics and Space Engineering. Student Member AIAA.

†Research Associate, Department of Aeronautics and Space Engineering; currently National Research Council Research Fellow, NASA Ames Research Center, Moffett Field, CA 94035. Member AIAA.

‡Associate Professor, Institute of Fluid Science. Associate Fellow AIAA.

§Professor, Department of Aeronautics and Space Engineering. Associate Fellow AIAA.

Introduction

WHEN a space vehicle enters into the atmosphere of a planet during a space mission, the temperature in the shock layer formed over the vehicle becomes sufficiently high to emanate strong radiation. Such a strongly radiating flowfield is considered to have occurred in the past planetary missions, for example, the Pioneer Venus probes[1] and the Galileo probe.[2] A similar situation will likely occur in future missions, such as MUSES-C.[3]

To evaluate the heat load to the vehicle accurately in such flowfields, radiative transfer phenomenon must be accounted for. In such a strongly radiating flowfield, radiation affects flowfield properties, which, in turn, affect radiation. Consequently, the flowfield must be calculated to account for this coupling effect.

An accurate radiation calculation, however, needs to consider a large number of wavelength points because the absorption coefficient of the gas strongly depends on wavelength. For example, a detailed line-by-line calculation requires wavelength points on the order of 10^6. Note that the number of wavelength points is equivalent to the number of radiative transfer equations to be solved just for obtaining a radiative intensity at a certain location in a specified direction. Moreover, such radiation calculation is repeated many times at each point in the flowfield for obtaining a converged solution.

To reduce this vast computing time, multiband models have been developed.[4] Modern multiband models evaluate absorption coefficients using wavelength points on the order of 10^3. These models successfully reduced the computing time of line-by-line calculation at least by a factor of 100 and reproduced the line-by-line result within a small error.[4]

To couple the radiation with the flowfield, either the so-called loosely coupled method or the fully coupled method is employed. In the loosely coupled method, radiation is updated once for a certain number of time steps. In the fully coupled method, radiation is updated for every time step. When radiation is not strong, a converged solution can be obtained by the loosely coupled method. When radiation is strong, however, strong interaction will occur between radiation and the flowfield. To obtain a converged solution for strongly radiating flowfield, a fully coupled method must be used.

Although loosely coupled calculations using a multiband model have been carried out,[5,6] they still required a considerable amount of computing time. In such calculations, a radiative transfer equation

was solved using the tangent-slab approximation. When radiation is strong, however, radiative heat transfer from the stagnation region can raise the temperature in the downstream region. In this event, one needs to account for multidimensional radiative transfer.

Sakai[7] has developed a new radiation model called the Planck–Rosseland–gray (PRG) model. In the PRG model, radiative intensities are calculated using dynamically assigned three mean Planck, Rosseland, and gray absorption coefficients, that is, the gas means. This model can reduce the computing time of the multiband model at least by a factor of 10 and closely reproduce radiative heat flux values obtained by line-by-line calculation. With this model, a fully coupled calculation with multidimensional radiative transfer was shown to be practical.

Tsuru and Sawada[8] showed that a converged solution could be obtained for a strongly radiating flowfield by applying the lower–upper symmetric Gauss–Seidel (LU-SGS) algorithm for solving the flowfield implicitly, whereas the radiative heat flux was integrated fully explicitly. Because of the explicit treatment of the radiative heat flux, the computing time, as well as the amount of computer memory required in the calculation, was substantially reduced. Fully coupled calculation of a strongly radiating flowfield with a multidimensional radiative transfer became very practical.

However, the use of the PRG model in the radiation calculation has an obvious shortcoming in that it needs to be calibrated once for every certain number of time steps to obtain a correct heat flux value at the solid wall. Calibration of the model is usually made by referring to the solution of the multiband model. Therefore, the fully coupled calculation cannot be carried out solely by use of the PRG model.

In this study, we consider the problem of a hypersonic strongly radiating flowfield over a hemisphere that was studied by Howe and Viegas using a shock-layer solution in equilibrium air and that employed a tangent-slab approximation for the radiative transfer calculation.[9] Instead of using these numerical methods, we try to achieve a fully coupled calculation of this strongly radiating flowfield with a multidimensional radiative transfer by choosing an alternative approach, that is, to employ a detailed multiband model in the radiation calculation directly. To reduce the substantial increase in computing time due to the use of the multiband model, a parallel computation is attempted. The purpose of the present study, therefore, is to demonstrate the feasibility of a fully coupled and spectrally detailed calculation of a strongly radiating flowfield using a multiband model with multidimensional radiative transfer, if we resort to parallel computations.

Formulation

Numerical Method

The governing equations are the axisymmetric Euler equations that can be written as

$$\frac{\partial Q}{\partial t} + \frac{\partial F}{\partial x} + \frac{\partial G}{\partial y} + H = H_{\text{rad}} \tag{1}$$

In the present study, the gas is assumed to be in thermochemical equilibrium. There are 11 chemical species, N, O, N_2, O_2, NO, N^+, O^+, N_2^+, O_2^+, NO^+, and e^-, considered in the flow calculation. The equilibrium gas properties are calculated by the free-energy minimization technique.[10] This technique is implemented through a table lookup interpolation method.[11]

A finite volume approach is used to discretize the governing equations. The AUSM-DV scheme is used to obtain the numerical convective flux.[12] The spatial accuracy is improved by the MUSCL approach.

A matrix-free LU-SGS method is employed for time integration.[13] In the time integration, the flowfield is integrated implicitly, whereas radiation is integrated explicitly.[8]

In the present calculation, a multidimensional radiative transfer is considered. The radiative heat flux is calculated by assuming one-dimensional (tangent-slab) or two-dimensional approximations in the radiative transfer calculation, or by considering three-dimensional radiative transfer directly. Note that the obtained radiative heat flux is consistent with Eq. (1) only when the three-dimensional radiative transfer calculation is made. In one- or two-dimensional cases, the radiative heat flux is calculated by assuming a computational domain that is different from the axisymmetric flowfield. Details can be found in Refs. 7 and 14 and, therefore, are not provided here. Examples of multidimensional radiation rays are shown in Figs. 1a and 1b for two- and three-dimensional radiative transfer calculations, respectively. Rays are calculated at every 10 deg.

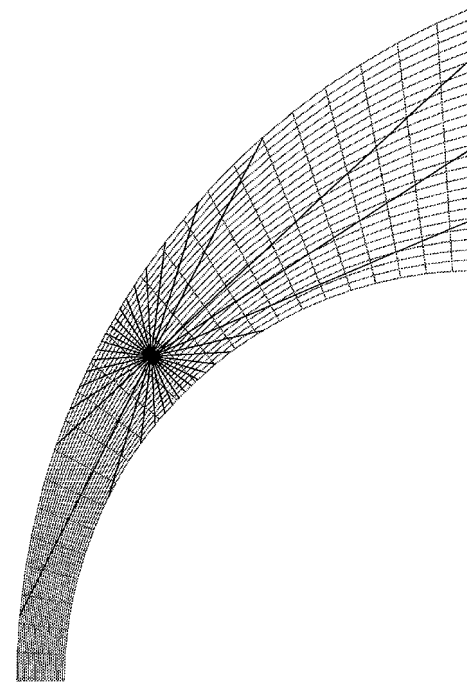

a) Two-dimensional radiation rays

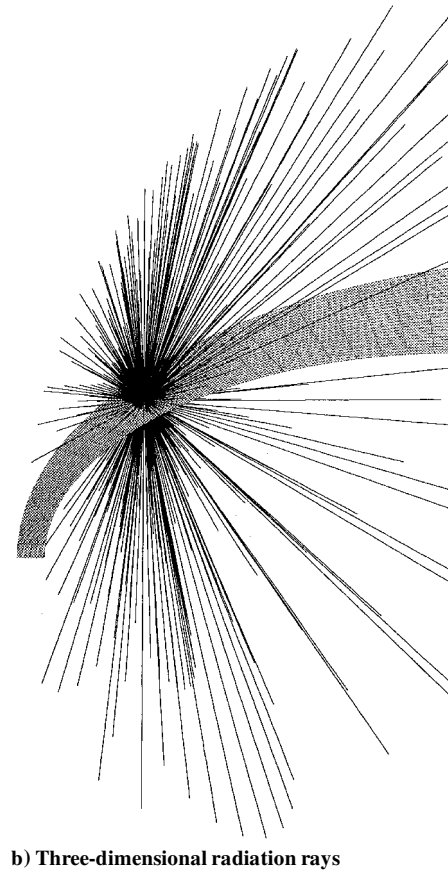

b) Three-dimensional radiation rays

Fig. 1 Example of multidimensional radiation rays.

Table 1 Radiation mechanisms involved in the present multiband model

Species	System
Atomic lines	
N	367 lines
O	103 lines
Molecular bands	
N_2	1^+, 2^+, LBH
O_2	SR
NO	β, γ
N_2^+	1^-
Bound-free continuum	
N	600–50,000 Å
O	500–10,000 Å

The absorption coefficients of a gas are calculated by the multiband model.[4] For air radiation, N, O, N_2, O_2, NO, and N_2^+ are considered. Radiation mechanisms involved in the calculation are summarized in Table 1. To obtain a converged solution for a strongly radiating flowfield, a fully coupled calculation is carried out.

Multiband Model

In this study, absorption coefficients are evaluated at 2294 wavelength points for the wavelength range from 750 to 15,000 Å. The absorption coefficient of a gas is expressed as a sum of those for individual species, written as[4]

$$\kappa_\lambda = \sum_i n_i \sigma_\lambda^i \tag{2}$$

The cross-section values are calculated for radiating species at 3000; 6000; 9000; 12,000; and 15,000 K based on a line-by-line technique. The cross-section value at a certain temperature is obtained by a curve fit in the following form:

$$\sigma_\lambda^i = \exp\left\{ A_{1\lambda}^i \Big/ z + A_{2\lambda}^i + A_{3\lambda}^i \ln(z) + A_{4\lambda}^i z + A_{5\lambda}^i z^2 \right\} \tag{3}$$

where $z = 10{,}000/T$ and $A_{k\lambda}^i$ $(k = 1, 2, 3, 4, 5)$ are fitting parameters.

Parallel Implementation

An important issue in the parallel computation is how to divide the computational loads and assign them to multiple processors. A division of the computational domain is usually employed for this purpose. In the problem of radiative transfer, however, such a strategy is hardly acceptable because a radiative heat flux value at a computational cell depends on the entire computational domain. If we divide the computational domain into multiple regions, information exchanges between divided computational regions become complicated. Moreover, it is difficult to achieve a uniform load distribution because the computational load differs with mesh location.

In the present study, we employ a division in wavelength range of a multiband radiation model. That is, we divide the wavelength range into groups and assign them to each processor. Note that the radiative transfer equation for a given wavelength can be calculated individually. The total radiative heat flux can be obtained by a sum of those radiative heat fluxes calculated on n processors as

$$\begin{aligned} q_{\text{rad}} &= \int_\lambda q_\lambda \, d\lambda \\ &= \int_{\lambda_1} q_\lambda \, d\lambda + \cdots + \int_{\lambda_i} q_\lambda \, d\lambda + \cdots + \int_{\lambda_n} q_\lambda \, d\lambda \\ &= q_{\text{rad},1} + \cdots + q_{\text{rad},i} + \cdots + q_{\text{rad},n} \end{aligned} \tag{4}$$

where $q_{\text{rad},i}$ is a radiative heat flux for a specified wavelength range calculated on the ith processor. The computational load for each wavelength is identical for all of the processors and, thus, easily achieves a uniform load distribution.

In the present calculation, we parallelize only the radiation calculation part of the heat flux because the computing time for updating the flowfield is negligibly small. Parallelization of the code is implemented through the shared-memory-type parallelization using OpenMP directives. The present parallel computation is carried out using up to 128 processors on the SGI ORIGIN 2000.

Flow Conditions

In the present study, calculations are conducted for the flowfield over a hemisphere with a radius of up to 1.524 m. We assume airflow is at an altitude of 57.9 km. The flow velocity is 15.24 km/s. The freestream temperature and the pressure are 252.8 K and 30.4 N/m^2, respectively. Under these conditions, the pressure becomes about 1 atm at the stagnation region. This justifies the assumption of thermochemical equilibrium.

Let us estimate the equilibration distances behind the shock wave more precisely and confirm the preceding justification. Park estimated the equilibration distance from the results of tests for nonequilibrium air carried out in a shock tube.[15] The maximum shock velocity attained in the experiment was 10 km/s. For shock velocity of 10 km/s, the characteristic parameter τp_∞ that gives the equilibration distance behind the shock wave is about 10^{-4} μs $\cdot$ atm. If we adopt the same value for a shock velocity of 15 km/s, the estimated equilibration distance becomes about 5 mm, whereas the shock standoff distance is about 60 mm for the radius of 1.524 m. Therefore, the shock layer is mostly in equilibrium. If we assume the radius to be 0.3048 m, the shock standoff distance becomes 14 mm (shown later). For this case, the equilibration distance becomes about one-third of the standoff distance, and, thus, the equilibrium assumption breaks down. However, the characteristic parameter of 10^{-4} is a conservative value for shock velocity of 15 km/s, and we can expect the equilibration distance most likely to be one order shorter than the shock standoff distance for this smaller-radius case.

With the preceding flow conditions, radiation from the flowfield becomes so strong that a fully coupled calculation is required for obtaining a converged solution. We have chosen these particular flow conditions for demonstrating robustness and the capability of the present computational fluid dynamics (CFD) code. This problem was studied by Howe and Viegas using a shock-layer solution in equilibrium air and a tangent-slab approximation.[9]

Figure 2 shows the fine computational mesh (51 × 51 grid points) used in the calculation. This fine mesh is used when either a one- or two-dimensional approximation of the radiative heat transfer calculation is employed, whereas a coarse mesh (26 × 26 grid points) is used when the three-dimensional radiative heat transfer is considered.

The boundary conditions for the flowfield calculation are assumed as follows: A slip condition is used at the wall, a symmetry condition

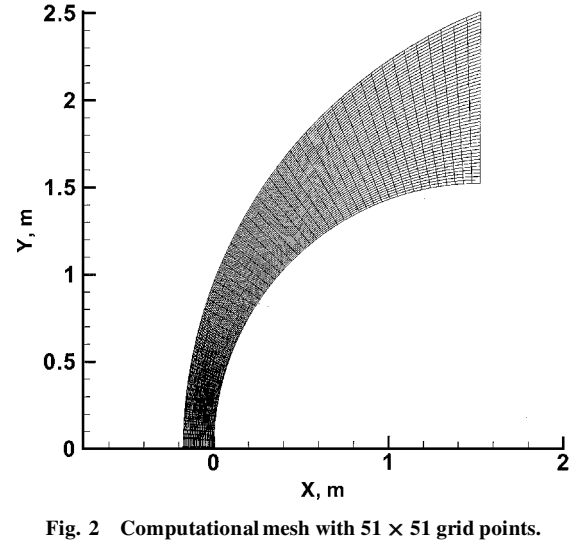

Fig. 2 Computational mesh with 51 × 51 grid points.

exists along the symmetry axis, a freestream condition exists at the inflow boundary, and zeroth-order extrapolation is used at the outflow boundary.

The boundary conditions for radiation calculation are as follows: The wall is assumed to be a blackbody of 3000 K, which is a typical temperature of an ablating wall, though ablation is not included in this study. Note that radiation from the assumed blackbody of 3000 K has a minor influence on the obtained result because radiation from the shock layer is far more dominant. The far field is also assumed to be a blackbody of freestream temperature. The radiative intensity from the outflow boundary is assumed to be zero.[16]

Results and Discussion

Computed Results

In the present study, calculations are carried out with a Courant–Friedrichs–Lewy (CFL) number up to 1000 in the radiation coupled calculation. This radiation coupled calculation is started from the uncoupled converged solution in which radiation is totally omitted.

Let us first show the results obtained for a hemisphere of 1.524-m radius. Figure 3 shows the convergence histories of the residual. The residuals slightly oscillate for all cases, but show a converging trend and decrease by more than five orders of magnitude within 2000 time steps.

Figure 4 shows the convergence histories of the wallward radiative heat flux at the stagnation point. The asymptotic values are obtained within 200 time steps for all cases. The radiative heat flux value utilizing a one-dimensional approximation of the radiative transfer is higher than that obtained for the two- or three-dimensional radiative transfers due to the assumed infinite slab layer in the radiative transfer calculation.

Figure 5 shows the calculated temperature contours with the three-dimensional radiative transfer. The temperature contours given by the one- or two-dimensional approximations of radiative transfer

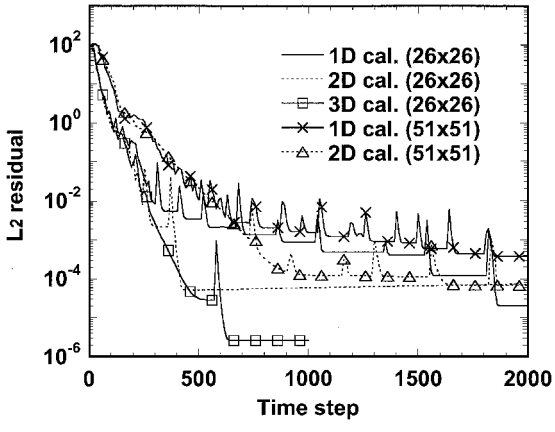

Fig. 3 Convergence histories of residuals for 1.524-m radius.

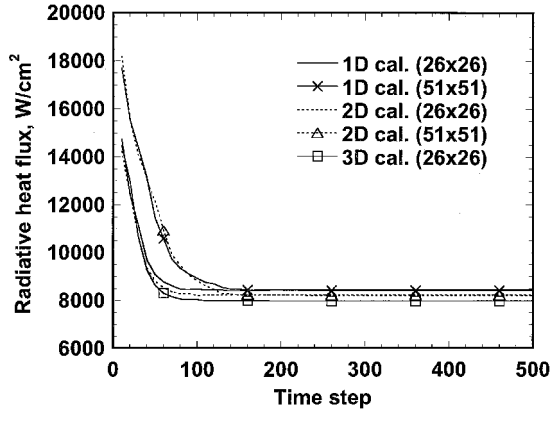

Fig. 4 Convergence histories of wallward radiative heat flux values at the stagnation point.

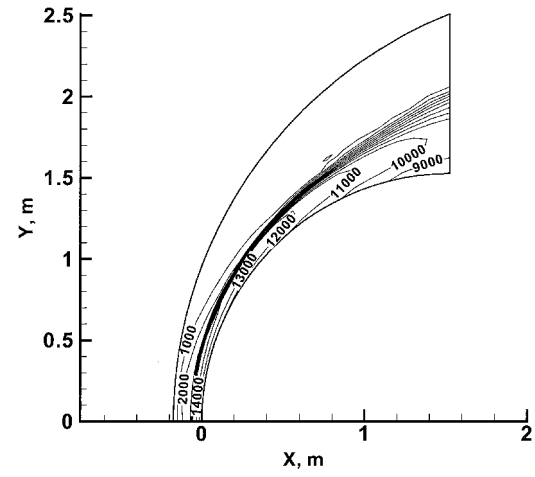

Fig. 5 Calculated temperature contours for 1.524-m radius; three-dimensional radiative transfer is considered.

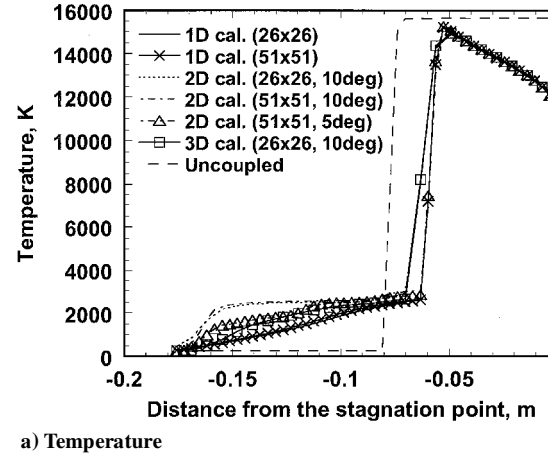

a) Temperature

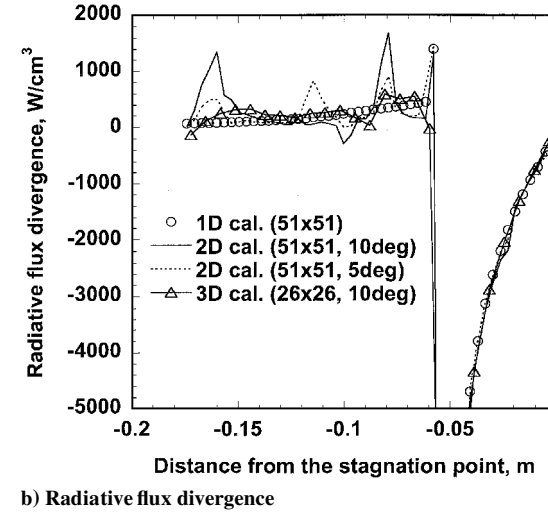

b) Radiative flux divergence

Fig. 6 Obtained profiles along the stagnation streamline for 1.524-m radius.

are almost identical in Fig. 5. As can be seen, a precursor heating appears ahead of the shock wave.

In Fig. 6a, the comparison of the temperature distributions along the stagnation streamline between the coupled and uncoupled calculations is shown. Note that the shock standoff distance is shorter than that for the uncoupled calculation because the shock-layer temperature is decreased by radiative cooling effects. The temperature profiles in the precursor region show some differences, depending on the approximation for the radiative transfer calculation, though the mesh convergence of the solutions utilizing the one- or

two-dimensional approximations of the radiative transfer calculation is well attained. In particular, the precursor heating becomes significant in the two-dimensional approximation.

To find the possible reason for the observed discrepancy in the precursor region, we have checked the behavior of radiative flux divergence along the symmetry axis. As shown in Fig. 6b, one can see that the two-dimensional radiative transfer calculation with radiation rays at 10-deg intervals gives a spiked profile at several locations in the precursor region where radiative flux divergence is substantially increased. If we employ a set of fine radiation rays at 5-deg intervals, then we have a smoother profile. These spikes in the two-dimensional case appear when a particular radiation ray comes to cross the region just behind the shock wave where the temperature is very high. Though the situation is the same for the three-dimensional case, such an effect is only significant in the two-dimensional case because the contribution from one radiation ray is much larger than that in the three-dimensional case. Also note that this effect is only noticeable when the computational cell is outside of the shock layer. The radiative flux divergence inside the shock layer does not show a spiked profile and the resulting temperature profile agrees well with that given by the one- or three-dimensional calculations.

It is now clear that obtaining a mesh convergence in terms of radiation rays is particularly important in the two-dimensional case. In this respect, the mesh convergence in the precursor region is not guaranteed for the present two-dimensional solution shown in Fig. 6a, which uses fine radiation rays. However, a fair agreement of the temperature profile with those of the one- and three-dimensional solutions in the precursor region suggests the obtained two-dimensional solution using fine radiation rays is virtually mesh converged. Once the convergence in terms of the radiation rays is reached, the present two-dimensional solution seems sufficiently accurate.

Figures 7a and 7b show the wallward radiative heat flux distributions along the body surface. The radiative heat fluxes monotonically decrease from the stagnation region to the downstream region. The radiative heat flux values that consider the two- or three-dimensional radiative transfers are consistently lower than those that employ the one-dimensional approximation. Note that the mesh convergence is shown in the wallward radiative heat flux profiles even for two-dimensional calculations using a different set of radiation rays.

Next, solutions are shown for a hemisphere of 0.3048-m radius. Because of the vast computing time required in the three-dimensional radiative transfer calculation, only the results utilizing the one- or two-dimensional approximations of the radiative transfer calculation are shown for this case. The convergence histories and temperature contours for this case are found to be almost identical with those for the 1.524-m-radius case and, therefore, are omitted.

The temperature distributions along the stagnation streamline are shown in Fig. 8. The effect of decreasing nose radius can be seen in Fig. 8. Although the shock standoff distance is also shorter than that for the uncoupled calculation, the radiative cooling effect and precursor heating become less significant in this case.

Figure 9 shows the wallward radiative heat flux distributions along the body surface. Also, in this case, the radiative heat flux values that consider the two-dimensional radiative transfer are consistently lower than those employing the one-dimensional approximation. The radiative heat flux values are smaller than those shown in Fig. 7 for the larger radius case.

Figure 10 shows the comparison of the shock standoff distances obtained by the present calculation with those obtained in previous studies.[8,9] In this study, the shock location is determined by first fitting the pressure profile near the shock wave using a spline curve and then finding the location where the maximum gradient occurs. One can see that the shock standoff distance obtained in the present calculation is identical with that which appeared in Ref. 8, but slightly shorter than that obtained in Ref. 9. Note that the numerical method

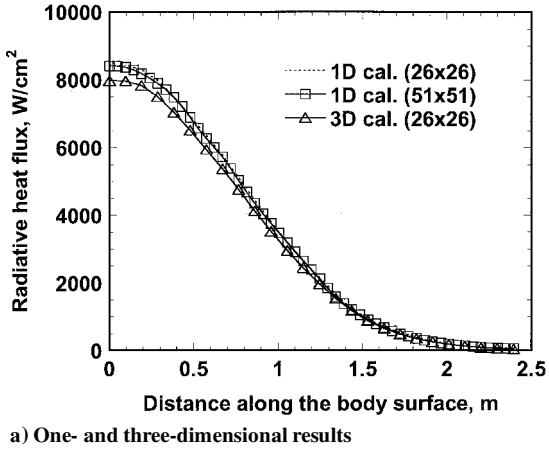

a) One- and three-dimensional results

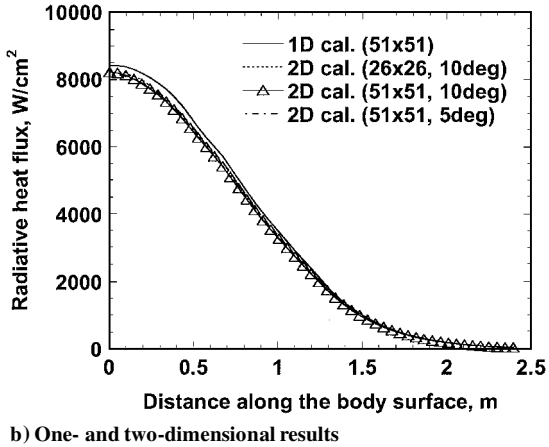

b) One- and two-dimensional results

Fig. 7 Comparison of radiative heat flux distribution along the body surface for 1.524-m radius.

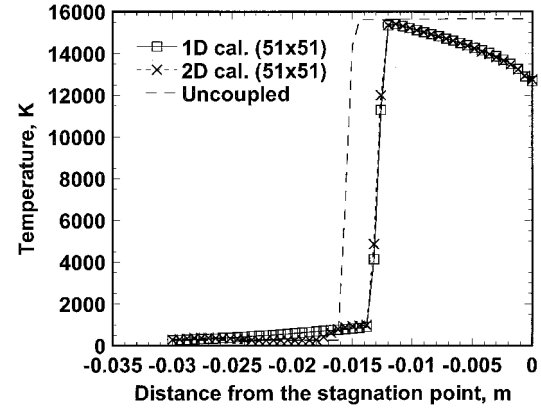

Fig. 8 Temperature distributions along the stagnation streamline for 0.3048-m radius.

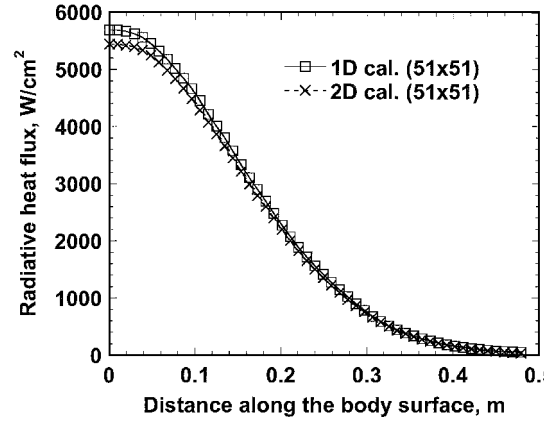

Fig. 9 Radiative heat flux distributions along the body surface for 0.3048-m radius.

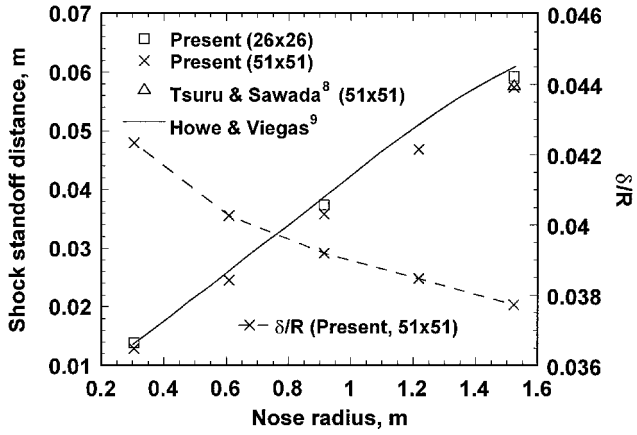

Fig. 10 Comparison of the shock standoff distance with those obtained in previous studies.[8,9]

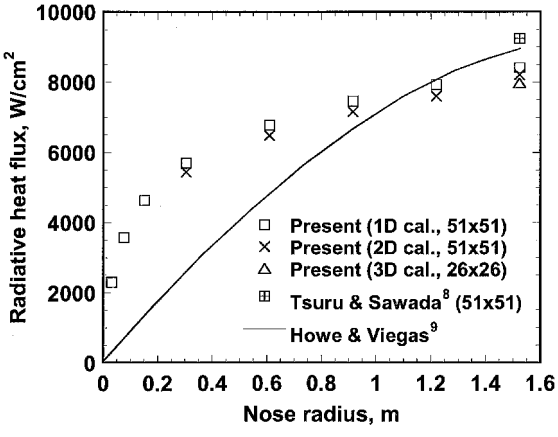

Fig. 11 Comparison of the wallward radiative heat flux at the stagnation point with those obtained in previous studies.[8,9]

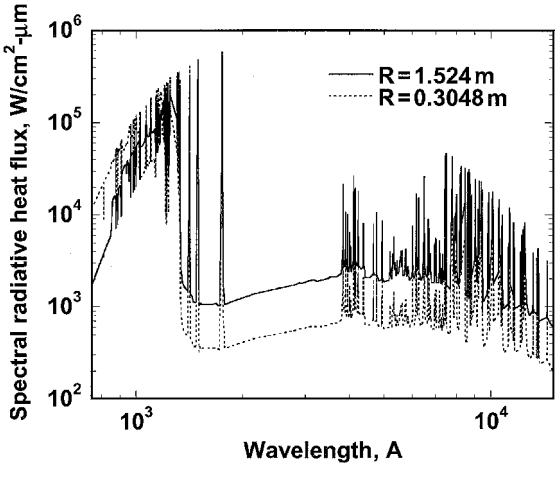

Fig. 12 Spectral wallward radiative heat flux at the stagnation point.

used in Ref. 8 is almost identical to the present calculation. It is seen from the ratio of shock standoff distance δ to sphere radius R (for the present 51×51 grid) that the reduction of the shock standoff distance due to the radiative cooling effect in the shock layer becomes significant with a larger radius.

The comparison of the wallward radiative heat fluxes at the stagnation point obtained by the present calculation with those obtained by the previous studies[8,9] is shown in Fig. 11. One can see that the present radiative heat flux value at the stagnation point gives a fair agreement with the existing result for a larger-radius case, but becomes substantially higher for the smaller-radius cases. Although a detailed comparison is difficult to make because the Planck mean absorption coefficient was used in Ref. 9, the cause of the higher radiative heat flux for the smaller-radius cases is examined.

In Fig. 12, the comparison of the spectral wallward radiative heat fluxes at the stagnation point is shown. Note that the spectral radiative heat flux for the 1.524-m radius becomes substantially larger than that for $R = 0.3048$ in the wavelength range longer than 1400 Å, but becomes comparable in the shorter wavelength range. The photon mean-free-path profiles evaluated at three different locations along the stagnation streamline, namely, behind the shock wave, at the middle of the shock layer, and at the stagnation point, are shown in Figs. 13a–13c. As is clearly indicated, the optical thickness of the shock layer is comparable to, or even shorter than, the shock standoff distance in the wavelength range shorter than 1400 Å, but far larger in the wavelength range longer than 1400 Å. Therefore,

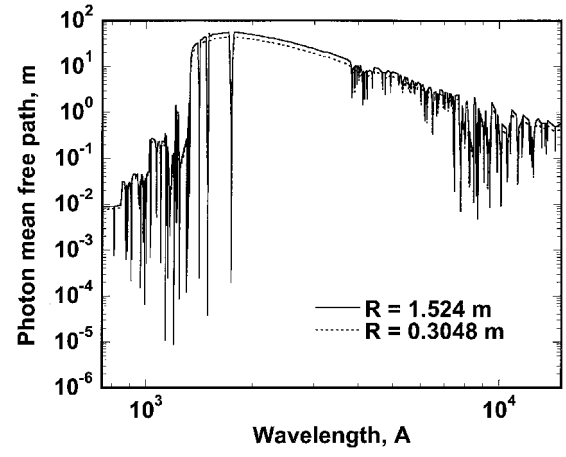

a) Behind the shock wave

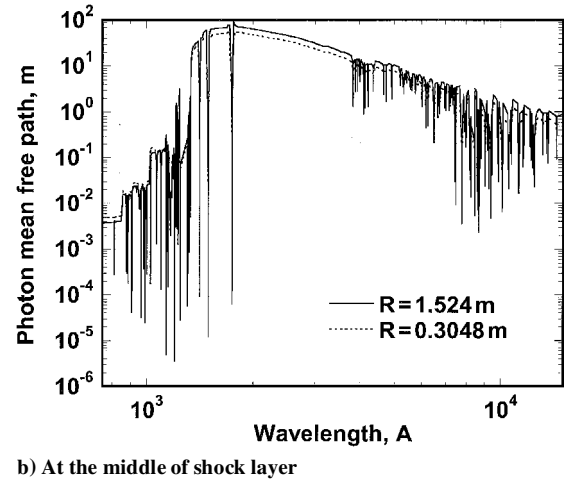

b) At the middle of shock layer

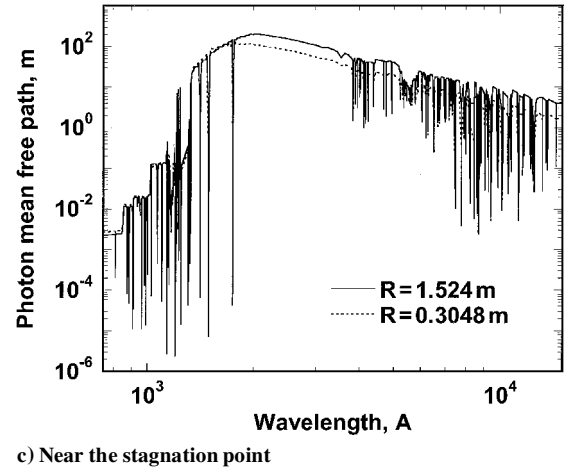

c) Near the stagnation point

Fig. 13 Photon mean free path around the stagnation region.

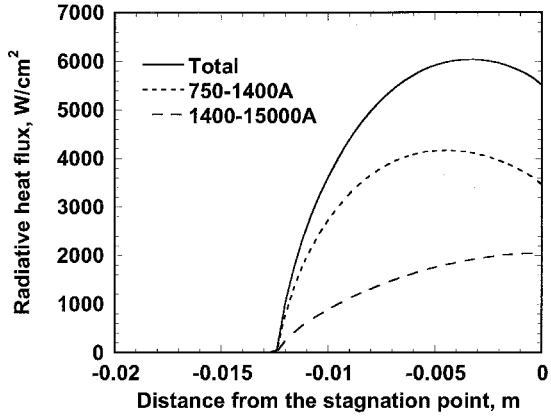

a) Radius of 0.3048 m

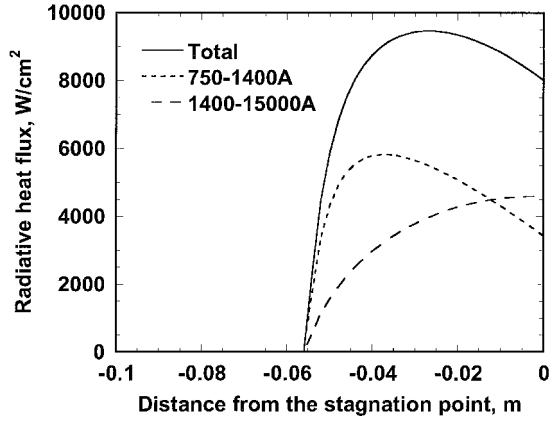

b) Radius of 1.524 m

Fig. 14 Radiative heat flux distributions along the stagnation streamline.

for smaller-radius cases, the radiative transfer from the wavelength region shorter than 1400 Å, which can be regarded as optically thick in the present shock layer, becomes dominant. This is well demonstrated in Figs. 14a and 14b, in which the total radiative heat flux profiles along the stagnation streamline are shown. Obviously, the contribution of the radiative heat flux from the shorter wavelength range is dominant for a smaller-radius case, whereas this contribution becomes less significant for a larger-radius case. From these considerations, we believe that the observed difference in heat flux value at the stagnation point for those smaller-radius cases comes from the difference in radiative properties of the shock-layer flow assumed in the radiative transfer calculations. Moreover, note that radiative heat transfer to a blunt body that has a smaller nose radius is shown to obey a different scaling law than that usually used for a transparent radiative shock layer in which radiative heat flux is directly proportional to the nose radius.[17]

Performance of Parallel Computations

In Figs. 15a and 15b, the obtained parallel performances are shown in terms of a relative speedup and parallel efficiency, respectively. Relative speedups achieved in the present calculations are fairly good for all cases. An almost linear scalability is achieved for the one-dimensional radiative transfer case. With 128 processors used, the one-dimensional radiative transfer calculation sustains a speedup ratio of 119 and a parallel efficiency of 93%. For the two-dimensional case, a speedup ratio of 100 and a parallel efficiency of 78% are obtained. For the three-dimensional case, we obtain a speedup ratio of 95 and a parallel efficiency of 74%. Those lower performances observed either in the two- or three-dimensional radiative transfer calculations are probably due to increased memory access through the network. In the present calculation, the radiation ray data set is stored in a global memory and shared among the processors. If we allocate the radiation ray data set on each local memory and exchange only flow properties by message passing, performance may be improved further.

Table 2 Required computing time and memory size for the calculation using 128 processors

Radiative transfer	Elapsed time, s	Memory, MB	GFLOPS
Coarse mesh (26 × 26 grid points)			
One-dimensional calculation	0.191	28.8	19.3
Two-dimensional calculation	4.55	103	22.0
Three-dimensional calculation	243	730	21.4
Fine mesh (51 × 51 grid points)			
One-dimensional calculation	0.612	75.0	21.4
Two-dimensional calculation	46.7	499	22.7

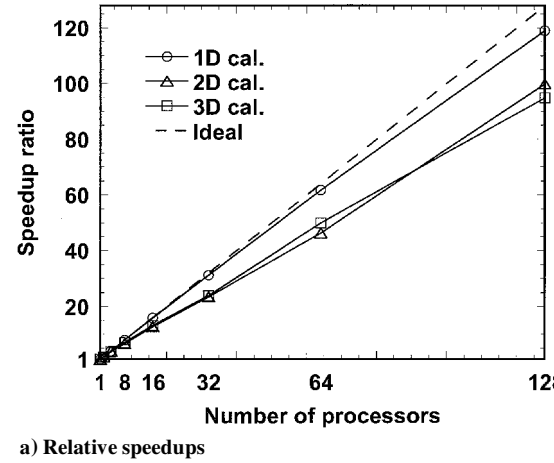

a) Relative speedups

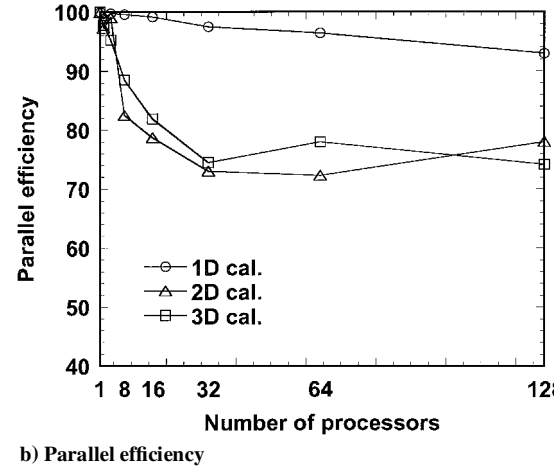

b) Parallel efficiency

Fig. 15 Parallel performance achieved in the present calculation.

Table 2 shows the required computing time per one time step and memory size for the calculation on 128 processors. In the present calculation, the parallel code achieves a computational speed of approximately 20 giga-floating point operations per second on 128 processors for all cases. For the calculation with three-dimensional radiative transfer, which is the most time-consuming case, it takes 243 s per one time step and requires 730 MB of memory. Obtaining the final solution takes about 67.5 h. If the same calculation is attempted on a single-vector supercomputer currently in use, the computing time may become more than 1000 h.

Conclusions

Parallel computation of a fully coupled hypersonic radiating flowfield is carried out using a spectrally detailed radiation model, accounting for multidimensional radiative transfer. A fair agreement of the shock standoff distance with that given by Howe and Viegas[9] is obtained for several different radii. However, the present result gives a substantially larger radiative heat flux value at the stagnation

point for smaller-radius cases. It is shown that the radiative transfer from the shorter wavelength region is optically thick in the shock layer and becomes dominant for smaller-radius cases. The strategy in parallel implementation of dividing the wavelength range is found to achieve good scalability. It is well demonstrated that a converged solution can be obtained in a feasible computing time if we resort to parallel computations.

Acknowledgment

All of the calculations are conducted on the SGI ORIGIN 2000 at the Institute of Fluid Science, Tohoku University.

References

[1]Pitts, W. C., and Wakefield, R. M., "Performance of Entry Heat Shields on Pioneer Venus Probes," *Journal of Geophysical Research*, Vol. 85, No. A13, 1980, pp. 8333–8377.

[2]Milos, F. S., "Galileo Probe Heat Shield Ablation Experiment," *Journal of Spacecraft and Rockets*, Vol. 34, No. 6, 1997, pp. 705–713.

[3]Ahn, H.-K., and Park, C., "Preliminary Study of the MUSES-C Reentry," AIAA Paper 97-0278, Jan. 1997.

[4]Park, C., and Milos, F. S., "Computational Equations for Radiating and Ablating Shock Layers," AIAA Paper 90-0356, Jan. 1990.

[5]Olynick, D. R., Henline, W. D., Chamber, L. H., and Candler, G. V., "Comparisons of Coupled Radiative Navier–Stokes Flow Solutions with the Project Fire II Flight Data," *Journal of Thermophysics and Heat Transfer*, Vol. 9, No. 4, 1995, pp. 586–594.

[6]Gökçen, T., and Park, C., "The Coupling of Radiative Transfer to Quasi 1-D Flows with Thermochemical Nonequilibrium," AIAA Paper 91-0570, Jan. 1991.

[7]Sakai, T., "The Computation of Strongly Radiating Hypersonic Flowfields," Ph.D. Dissertation, Dept. of Aeronautics and Space Engineering, Tohoku Univ., Sendai, Japan, Jan. 1999.

[8]Tsuru, T., and Sawada, K., "Convergence Issues on Fully-Coupled Radiative Gas Dynamic Calculations," AIAA Paper 2000-0732, Jan. 2000.

[9]Howe, J. T., and Viegas, J. R., "Solutions of the Ionized Radiating Shock Layer, Including Reabsorption and Foreign Species Effects, and Stagnation Region Heat Transfer," NASA TR-R-159, Jan. 1963.

[10]Gordon, S., and McBride, B. J., "Computer Program for Calculation of Complex Chemical Equilibrium Compositions, Rocket Performance, Incident and Reflected Shocks, and Chapman–Jouguet Detonations," NASA SP-273, Feb. 1971.

[11]Liu, Y., and Vinokur, M., "Equilibrium Gas Flow Computations I. Accurate and Efficient Calculation of Equilibrium Gas Properties," AIAA Paper 89-1736, June 1989.

[12]Wada, Y., and Liou, M. S., "A Flux Splitting Scheme with High-Resolution and Robustness for Discontinuities," AIAA Paper 94-0083, Jan. 1994; also NASA TM-106452, Jan. 1994.

[13]Nakahashi, K., Sharov, D., Kano, S., and Kodera, M., "Applications of Unstructured Hybrid Grid Method to High-Reynolds Number Viscous Flows," *International Journal for Numerical Methods in Fluids*, Vol. 31, No. 1, 1999, pp. 97–111.

[14]Sakai, T., Tsuru, T., and Sawada, K., "Computation of Hypersonic Radiating Flowfield over a Blunt Body," *Journal of Thermophysics and Heat Transfer*, Vol. 15, No. 1, 2001, pp. 91–98.

[15]Park, C., *Nonequilibrium Hypersonic Aerothermodynamics*, Wiley, New York, 1990, pp. 289–292.

[16]Hartung, L. C., and Hassan, H. A., "Radiation Transport Around Axisymmetric Blunt Body Vehicle Using a Modified Differential Approximation," *Journal of Thermophysics and Heat Transfer*, Vol. 7, No. 2, 1993, pp. 220–227.

[17]Anderson, J. D., Jr., *Hypersonic and High Temperature Gas Dynamics*, McGraw–Hill, New York, 1989, pp. 659–662.